Difracción de polvo y su aplicación en metalurgia

Oriol Vallcorba

Experiments Division
ALBA Synchrotron Light Source - CELLS (www.cells.es)
Carrer de la Llum 2-26, 08290, Cerdanyola del Vallès, Barcelona (Spain)
Phone: +34 93 592 4363 e-mail: ovallcorba@cells.es

ALBA

Aplicaciones del Sincrotrón ALBA a la Industria Metalúrgica y al tratamiento de superficies
Cerdanyola del Vallès, June 1st 2018

Outline

Introduction

X-ray Powder Diffraction

The MSPD beamline in ALBA

Applications to Metallurgy

Phase analysis

Microstructure

Texture

Powder Diffraction

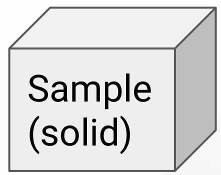

Periodical arrangement
of atoms ("crystal")

Infinite and periodic 3D arrangement of scatterers = **Crystal**

lattice

Atoms

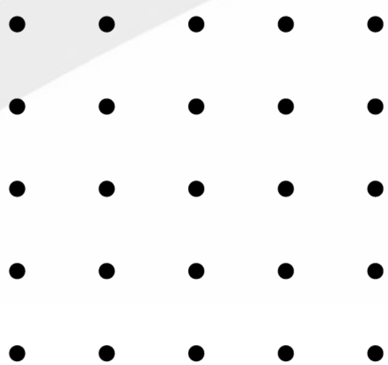

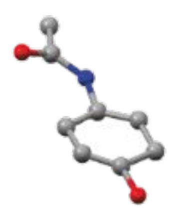

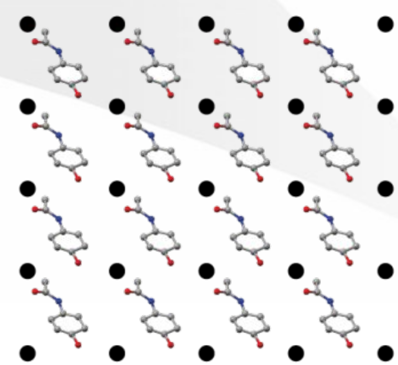

Powder Diffraction

Elastic scattering of the radiation beam (**diffraction**)

Radiation beam

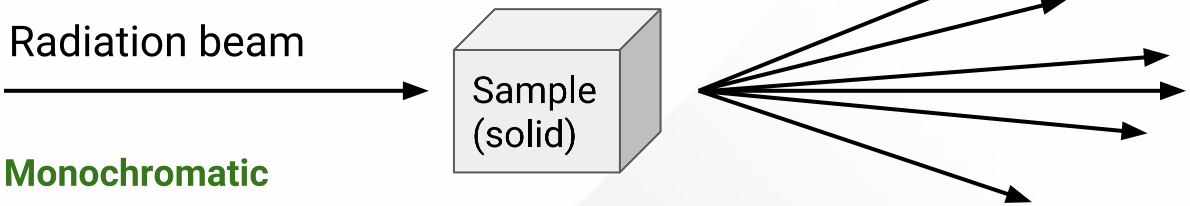

eg: **Monochromatic X-RAYS** case

Periodical arrangement of atoms ("crystal")

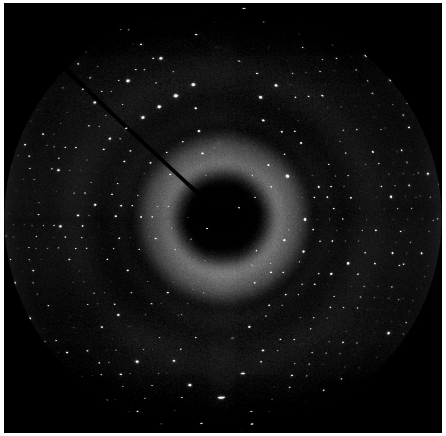

Diffracted beam spots ("reflections")

"sharp" peak case

At restricted angles (related with wavelength and crystal periodicity)

$$\mathbf{n\lambda = 2dsin\theta}$$

Powder Diffraction

Elastic scattering of the radiation beam (**diffraction**)

Radiation beam

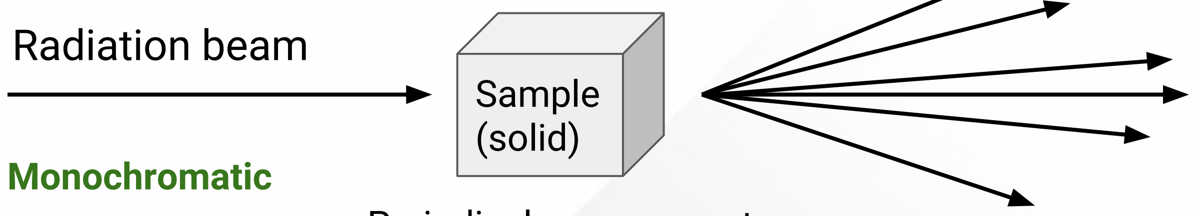

eg: **Monochromatic X-RAYS** case

Periodical arrangement of atoms ("crystal")

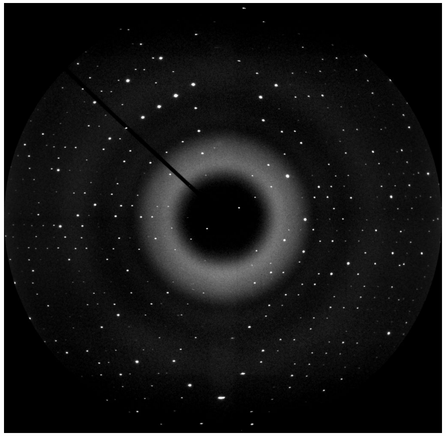

Diffracted beam spots ("reflections")

"sharp" peak case

At restricted angles (related with wavelength and crystal periodicity)

$$n\lambda = 2d\sin\theta$$

(Ewald construction)

diffracted beam (-120)

Incident beam

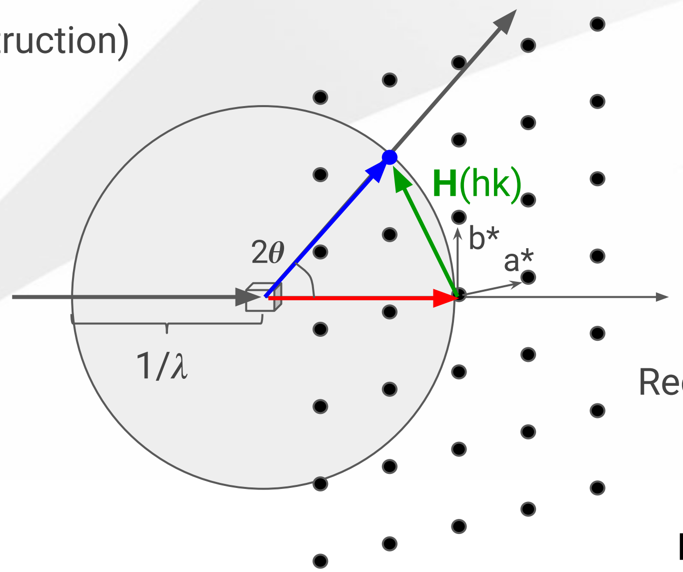

Reciprocal lattice

Rotate the crystal to get other Bragg reflections

Powder Diffraction

Single crystal or “grain”

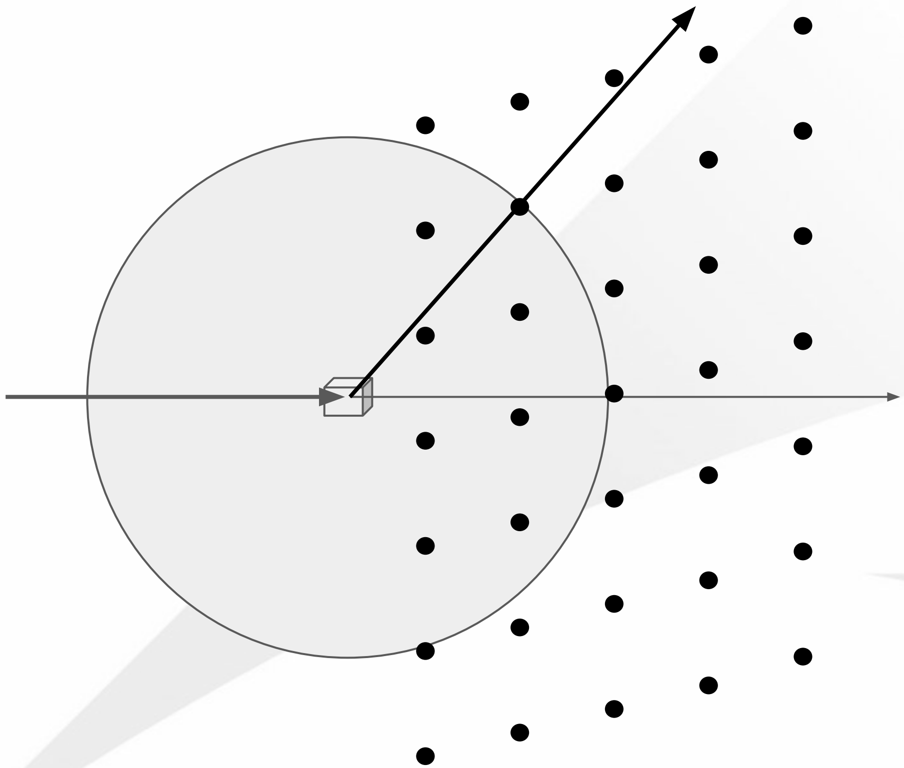

Powder Diffraction

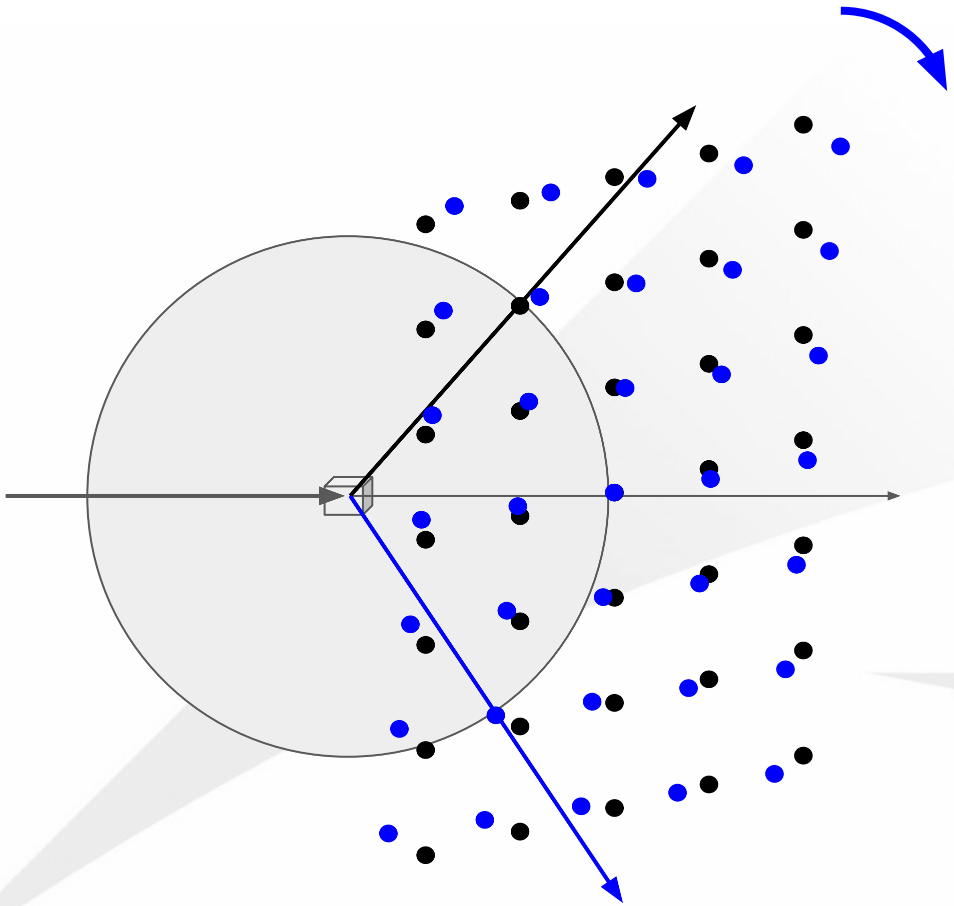

Same single crystal slightly rotated

or

2 grains with different orientations

Powder Diffraction

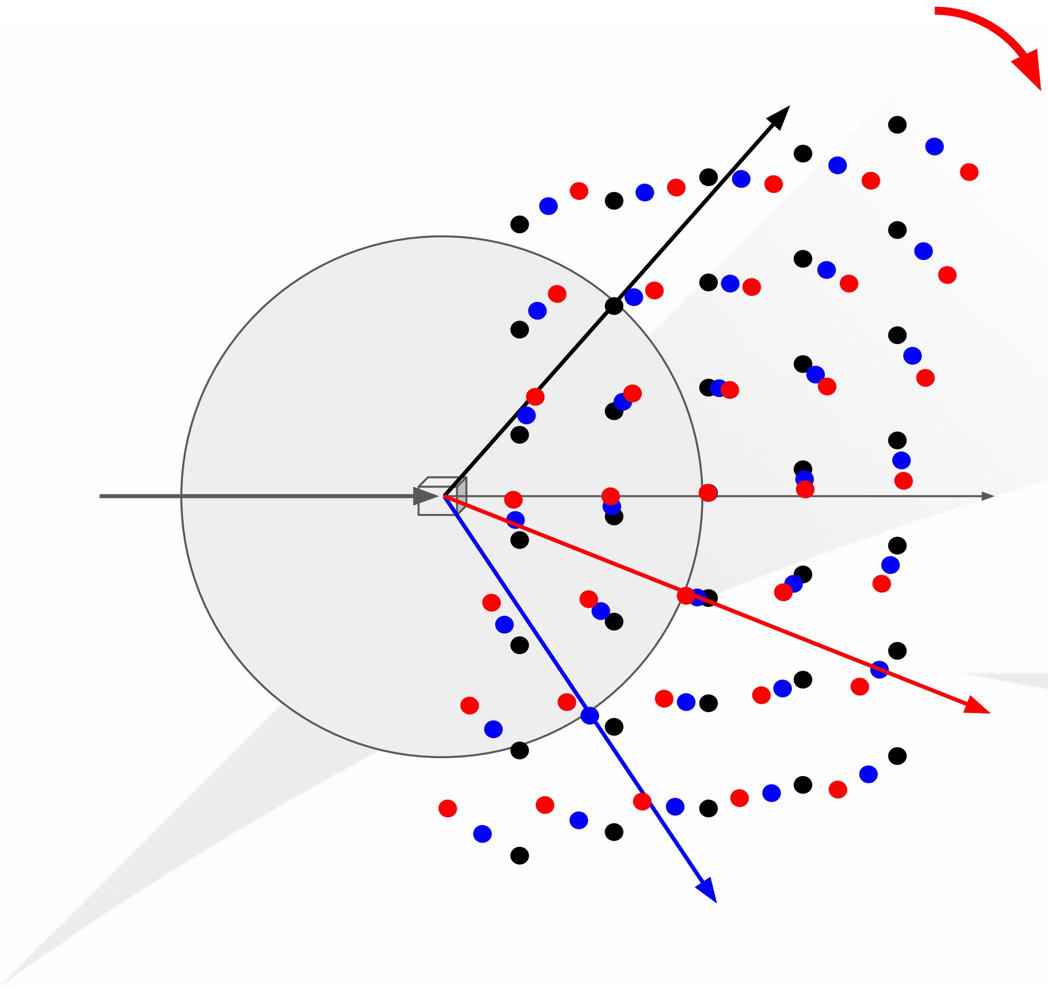

Same single crystal slightly rotated

or

3 grains with different orientations

Powder Diffraction

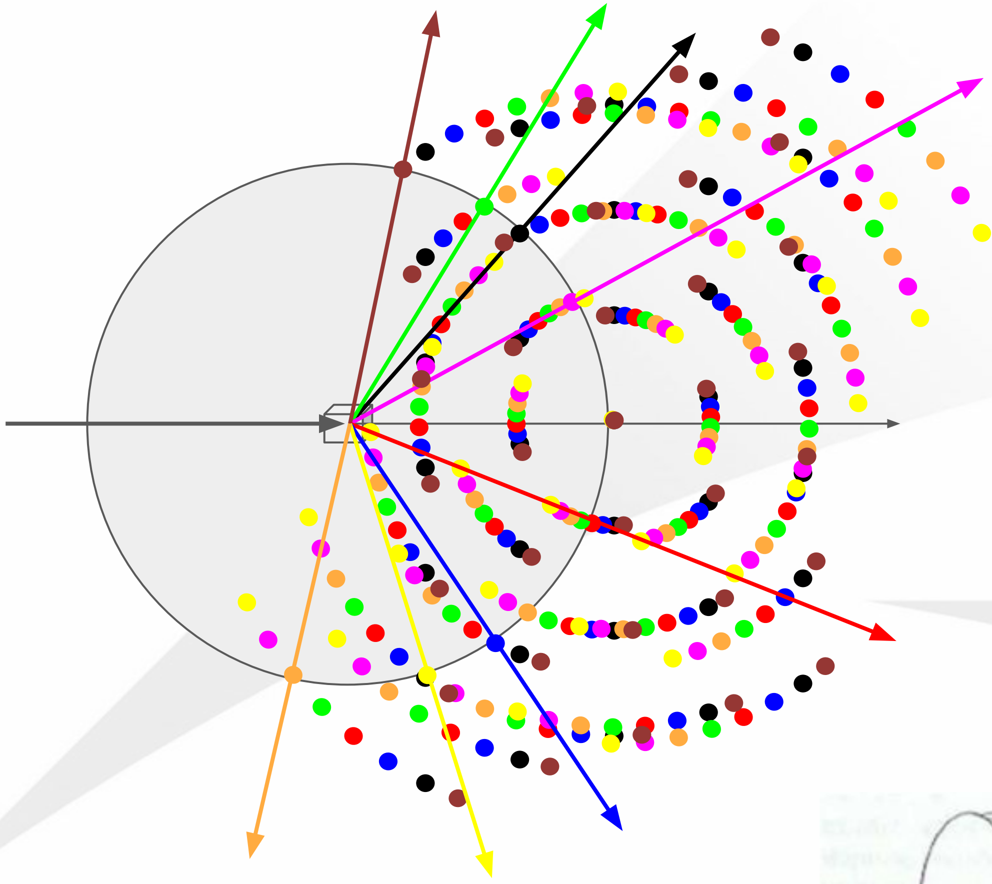

Same single crystal widely rotated

or

N grains with different orientations

Polycrystalline diffraction

(*aka* powder)

Diffraction is the superposition of all the contributing crystals

In 3D, the hkl Bragg peak is no longer a single spot, since all same hkl spots are at same 2θ, they lie on a **cone** (Debye-Scherrer cone)

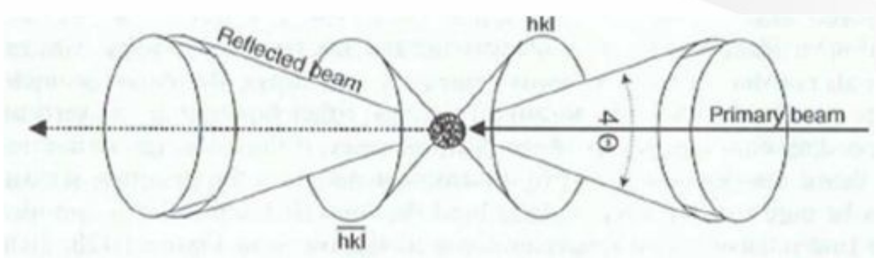

Powder Diffraction

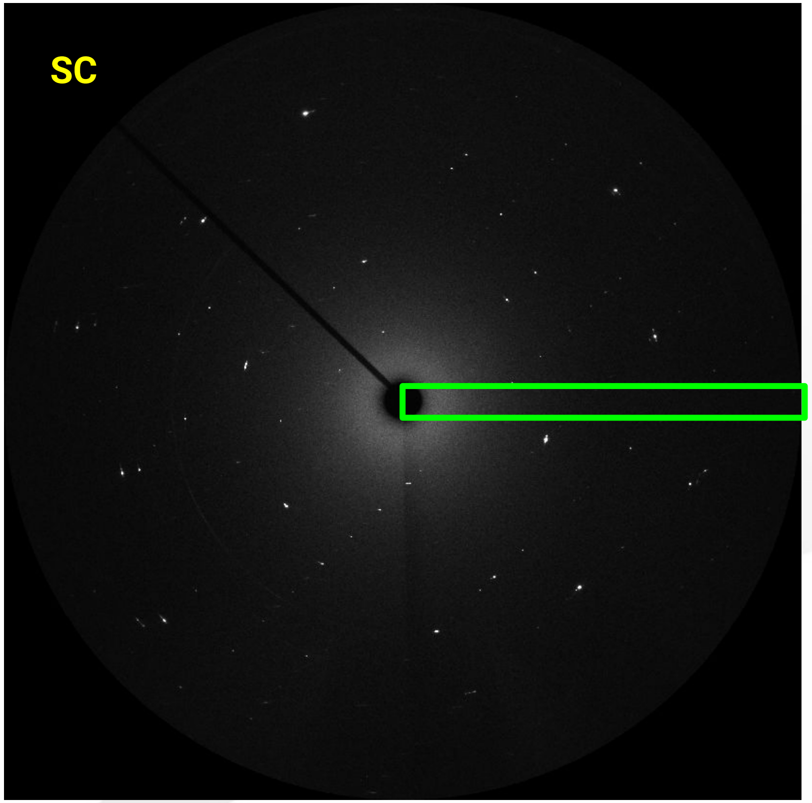

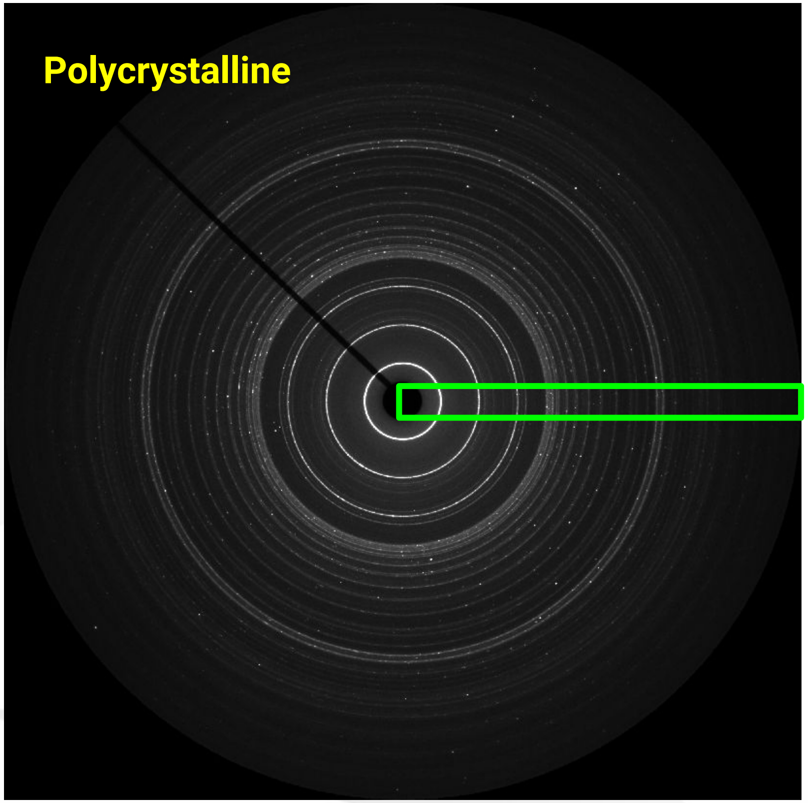

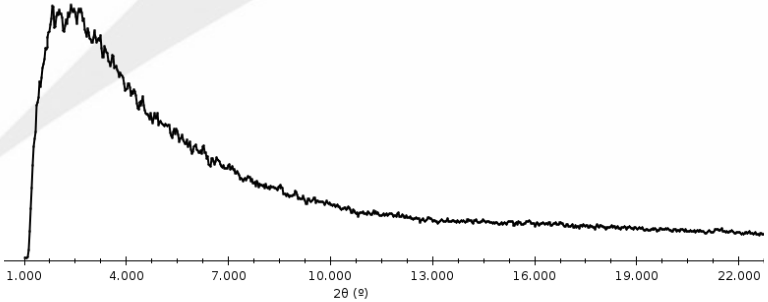

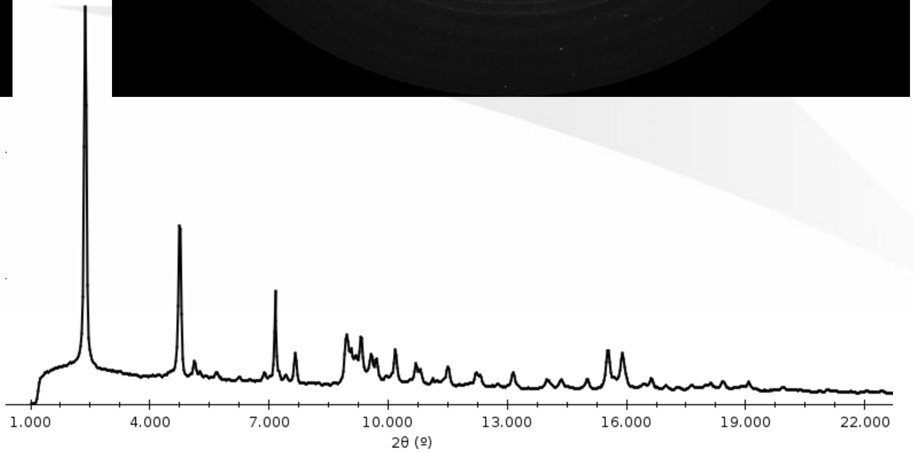

Powder Diffraction

Powder Pattern → "Peaks"

"Peaks" → Position → Lattice ($\lambda=2d_{hkl}\sin\theta_{hkl}$)

Cell parameters

Qualitative phase analysis

"Peaks" → Intensity → Kind and position of the atoms ($\boldsymbol{F_{hkl}}$)

Quantitative phase analysis

Crystal structure: atomic positions, occupancies, thermal factors, ...

"Peaks" → Profile function → Instrument contribution

Profile function → Microstructural features (strain, size)

Peak shape: Crystallite-size effects, dislocations, internal stresses,...

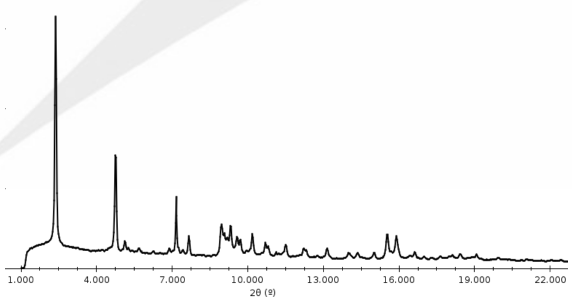

Powder Diffraction

- Powder Pattern
  - "Peaks"
    - Position → Lattice ($\lambda=2d_{hkl}\sin\theta_{hkl}$)
    - Intensity → Kind and position of the atoms ($\boldsymbol{F_{hkl}}$)
    - Profile function
      - Instrument contribution
      - Microstructural features (strain, size)
  - Background
    - Air/holder scattering
    - Sample
      - Compton scattering
      - Diffuse scattering

Cell parameters

Qualitative phase analysis

Quantitative phase analysis

Crystal structure: atomic positions, occupancies, thermal factors, ...

Peak shape: Crystallite-size effects, dislocations, internal stresses,...

Local structure information (PDF)

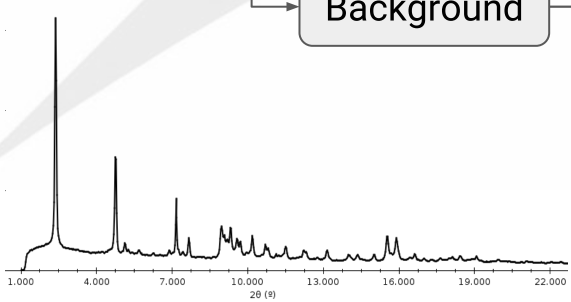

Powder Diffraction

Elastic scattering of the radiation beam (**diffraction**)

Radiation beam

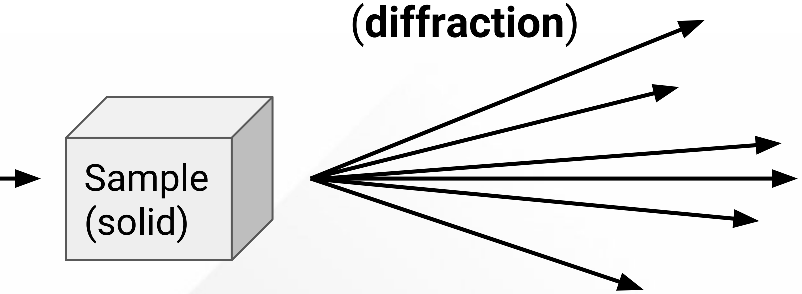

eg: **Monochromatic X-RAYS**

Periodical arrangement of atoms ("crystal")

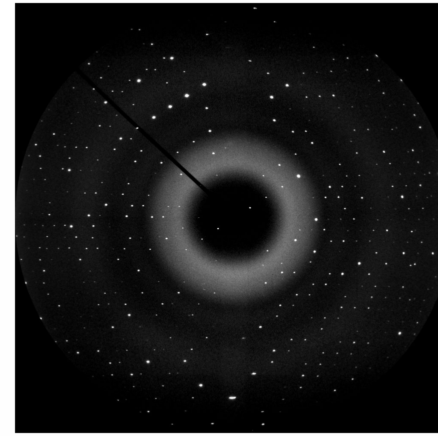

Diffracted beam spots ("reflections")

Obtain Structural Information

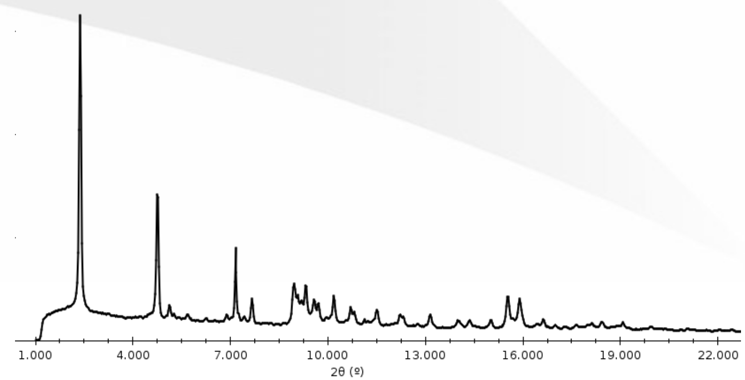

MSPD Beamline

High-Resolution Powder Diffraction endstation

- Transmission measurements (capillary)

  Position Sensitive (MYTHEN) or Multi-Analyzer (MAD)

- *In-situ* studies

  Temperature, batteries, catalysis,...

- Other specific measurement protocols

  e.g. Reflection mode (residual stress, thin films,...)

Sample Environment

- Hot air blower (300-950ºC)
- LN2 Cryostream (80-480K)
- LHe Cryostat (down to ~5K)
- Capillary flow cell
- Potentiostat
- Multispinner & coin-cell changer

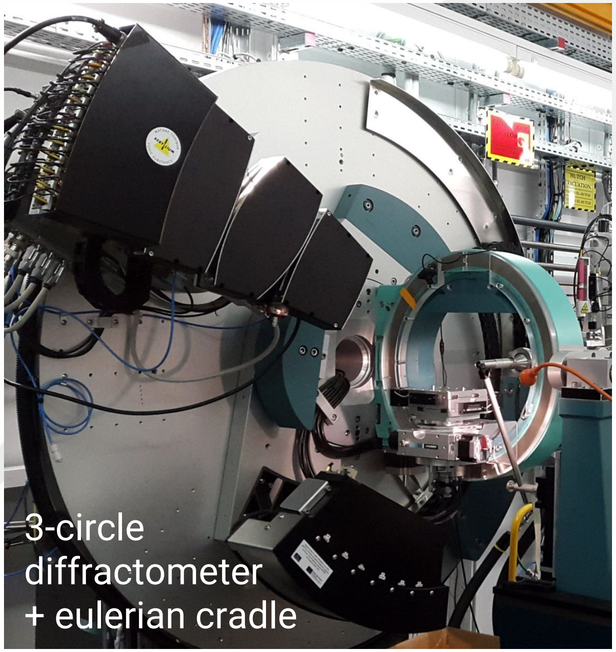

Multi Analyser Detector (MAD)

- 13 channels with 1.5º pitch
- Si111 or Si220 Bragg reflection
- YAP scintillator + PMT
- 10 to 50 keV

MYTHEN-II detector

- 6 modules (1280 channels, 50µm pitch)
- Sample to Det. dist. 550mm (40º 2θ in 0.005º pitch)
- ms time resolution
- 7 to 30 keV
- Up to Q~27 $Å^{-1}$ for total scattering exps. (120º/30keV)

MSPD Beamline

High-Pressure/µXRD endstation

- High-pressure experiments (DACs)
- Microdiffraction

  Free-standing, sc, cultural heritage, texture,...
- Other specific measurement protocols

  e.g. Non-KB, reflection, capillary cells, ...

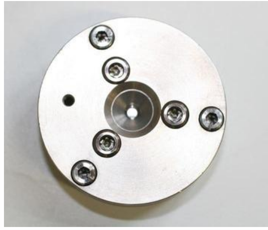

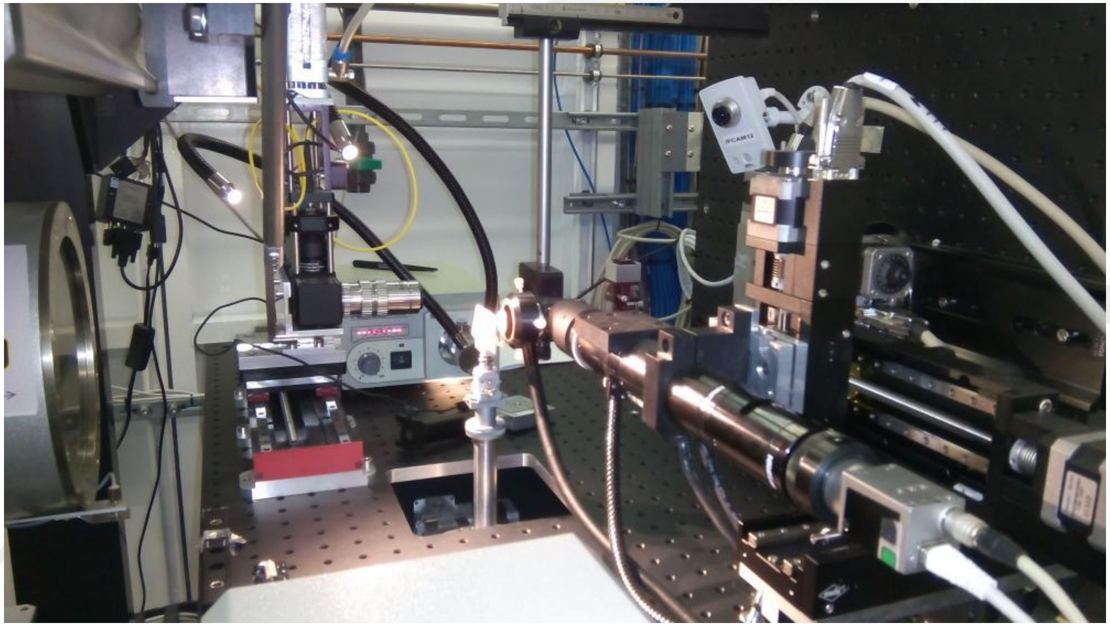

Kirkpatrick-Baez (KB) focusing optics

- Spot size of 15 x 15µm FWHM at sample position (20-50 keV)

Sample mounting/environment

- XYZ stage, omega (and chi)
- Diamond anvil cells (+ temperature)
- Spectrometer for online pressure calibration (Ruby)
- Online visualization system

CCD camera

- SX165 (Rayonix)
- Round area (Ø165mm)
- 20 to 50 keV
- Dynamic range 16 bit

Synchrotron X-ray diffraction advantages

High flux

Broad range of energies

Low natural beam divergence

Small spot size

Detector systems

Sample environments

Penetration of absorbing materials

Fast acquisitions (Time-resolved studies)

Good signal to noise, statistics

High angular resolution

Small amount of sample required

Measurement of small volumes

In-situ studies

Radiation damage

Grain size / Homogeneity

(powder diffraction)

Reflection experiments

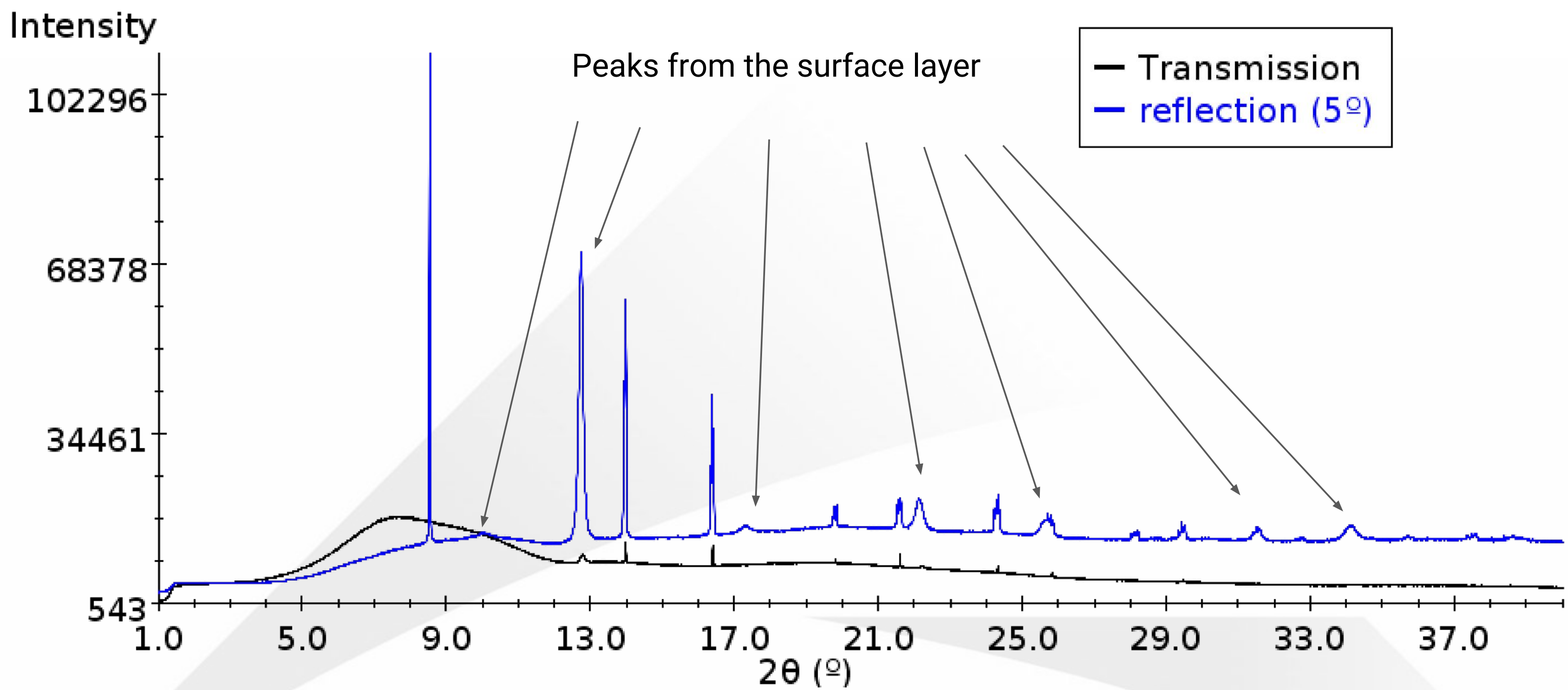

- For thick samples with high absorption
- For thin layers on “substrates”
- Improve the contribution of the surface
- Qualitative analysis

Applications in metallurgy

Qualitative and Quantitative phase analysis

Crystalline phases in the material

(peak position and intensity)

Microstructure

Particle size, stress

(peak width, shape and position)

Texture

Orientation of the material

(Intensities from certain families of reflections)

(influence on material properties)

Effects of Heat-Treatment Temperature on the microstructure of the $Ti_{50}Ni_{45}Cu_5$ alloy

- Optimization of internal friction and mechanical properties by using a suitable HTT.

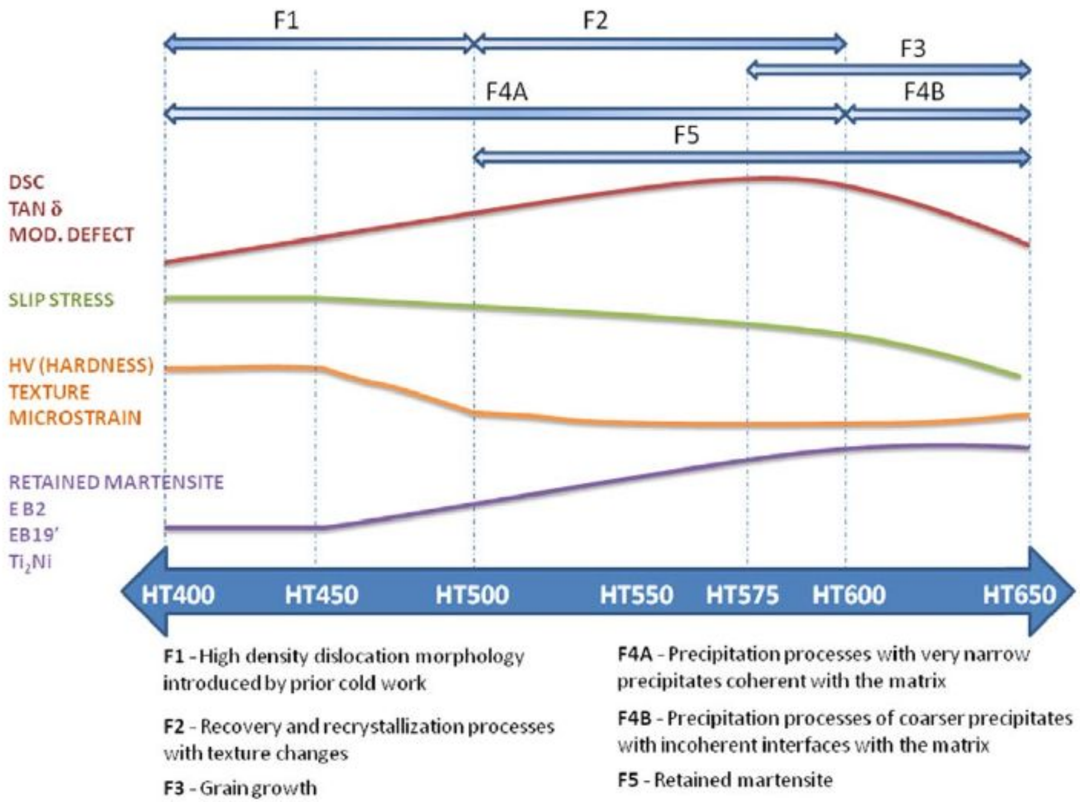

Summary of the tendencies of the studied properties with HTT and the correlation with the causing factors.

- PD to study changes that the HTT causes in the microstructure (crystallite size, wt% phases, microstrain and texture)

Identifying the effects of heat treatment temperatures on the $Ti_{50}Ni_{45}Cu_5$ alloy using dynamic mechanical analysis combined with microstructural analysis. A. Fabregat-Sanjuan, F. Gispert-Guirado, F. Ferrando, & S. De la Flor. *Materials Science and Engineering: A*, **2018**, 712, 281–291.

Effects of Heat-Treatment Temperature on the microstructure of the $Ti_{50}Ni_{45}Cu_5$ alloy

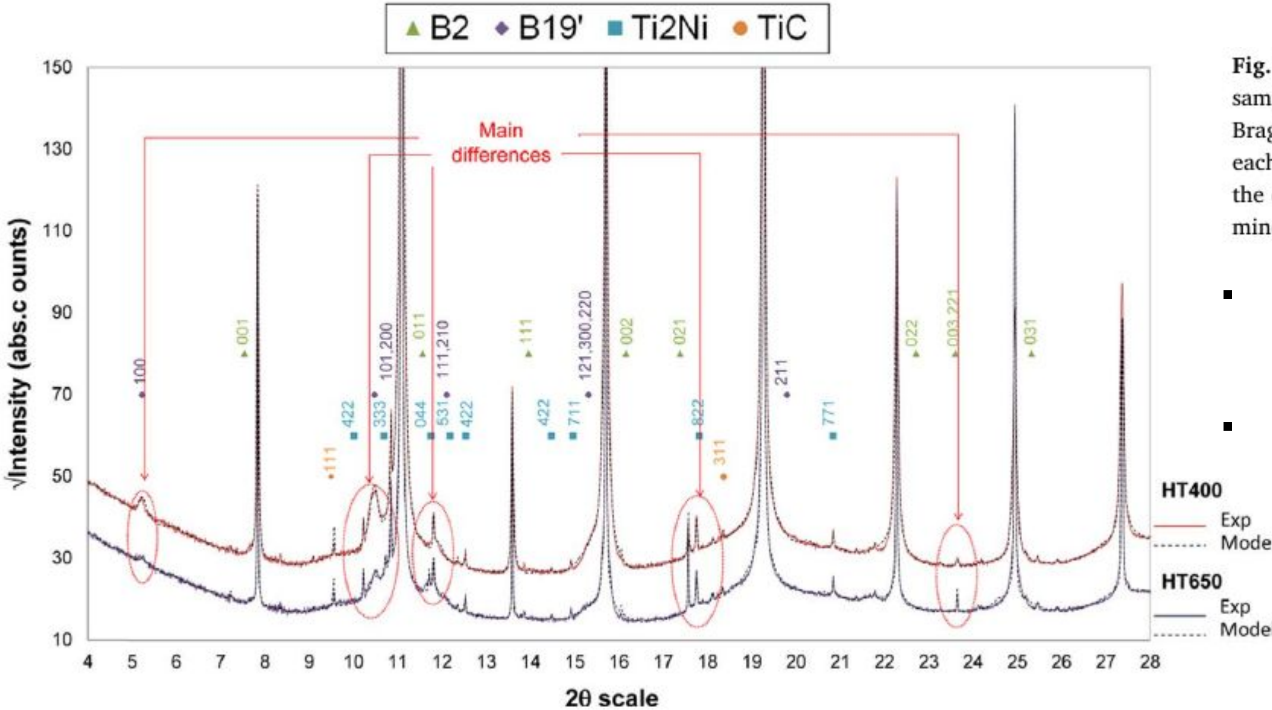

Fig. 7. Measured and calculated SXRD patterns for samples HT400 and HT650 at 120 °C. The main Bragg peaks with their *hkl* indexes are indicated for each phase. This plot shows the low intensity part of the diffractogram in order to reveal the peaks of the minor phases.

- Sample in **wires** measured in **transmission** (1mm diameter, 20mm length)
- **30Kev** to minimize absorption

Results of the relative quantitative analysis (in wt%) by the Rietveld method for the identified phases at 120 °C. Also shown is the conventional Rietveld agreement factor R_{wp}. n.d.: not detected.

Sample	NiTiCu-austenite (B2)	NiTiCu-martensite (B19′)	Ti_2Ni	TiC	$Cu_{0.9}TiNi_{1.1}$	R_{wp}
HT400	97.65 (0.19)	1.53 (0.18)	0.53 (0.03)	0.29 (0.03)	n.d.	8.43
HT450	97.80 (0.17)	1.41 (0.16)	0.57 (0.03)	0.22 (0.03)	n.d.	9.42
HT500	96.23 (0.24)	2.95 (0.24)	0.56 (0.03)	0.26 (0.03)	n.d.	9.35
HT550	95.07 (0.25)	3.2 (0.25)	0.63 (0.03)	0.28 (0.03)	0.82 (0.06)	8.66
HT575	93.85 (0.27)	4.52 (0.26)	0.67 (0.03)	0.23 (0.03)	0.73 (0.06)	9.4
HT600	91.83 (0.29)	6.77 (0.28)	0.62 (0.03)	0.29 (0.03)	0.49 (0.07)	8.83
HT650	92.49 (0.29)	6.58 (0.28)	0.60 (0.03)	0.33 (0.03)	n.d.	9.61

Effects of Heat-Treatment Temperature on the microstructure of the $Ti_{50}Ni_{45}Cu_5$ alloy

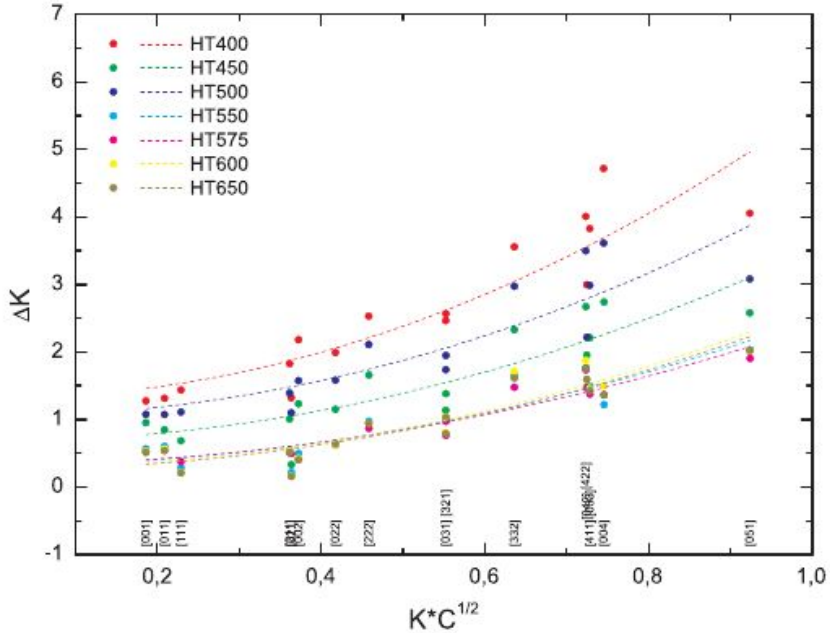

Fig. 8. Modified Williamson-Hall plot (dots) of the NiTi-austenite peaks measured at 120 °C for different temperatures of training: peak width (ΔK) v. peak position corrected by the average diffraction contrast factor $(K\overline{C}^{\frac{1}{2}})$.Dashed lines: fitted function in Eq. (1) from the dots. The Miller indexes (*hkl*) for each peak are indicated.

Table 4
Results of the texture index calculated from the preferred orientation correction by using the general spherical harmonics correction, apparent crystallite size (D_{hkl}, in nm), density of dislocations (α′) calculated with the modified Williamson-Hall plot (Fig. 8) for the NiTiCu-austenite phase, and the March-Dollase index for preferred orientation correction for NiTiCu-martensite phases and precipitates at 120 °C.

	NiTiCu-austenite (B2)			NiTi-martensite (B19′)	
Sample at 120 °C	Texture index	D_{hkl}	α′	March-Dollase index	D_{hkl}
HT400	1.145 (0.002)	39 (5)	4.3 (0.5)	1.19(0.06); 0.2(0.1)	6.4(0.3)
HT450	1.113 (0.002)	76 (6)	2.8 (0.4)	1.3(0.1); 0.2(0.2)	6.3(0.4)
HT500	1.139 (0.002)	49 (10)	3.3 (0.5)	1.6(0.1); 0.2(0.2)	6.4(0.4)
HT550	1.033 (0.001)	161 (17)	2.2 (0.3)	1.5(0.2); 0.2(0.4)	6.4(0.8)
HT575	1.023 (0.001)	156 (16)	2.1 (0.2)	1.2(0.2); 0.2(0.4)	6.4(0.8)
HT600	1.024 (0.001)	191 (20)	2.4 (0.3)	1.7(0.2); 0.2(0.3)	8.2(0.8)
HT650	1.030 (0.001)	206 (23)	2.3 (0.2)	1.4(0.1); 0.2(0.9)	12.7(2.0)

Identifying the effects of heat treatment temperatures on the $Ti_{50}Ni_{45}Cu_5$ alloy using dynamic mechanical analysis combined with microstructural analysis. A. Fabregat-Sanjuan, F. Gispert-Guirado, F. Ferrando, & S. De la Flor. *Materials Science and Engineering: A*, **2018**, 712, 281–291.

Intermetallic phases in Al-Cu joints

- Identify the IMC phases formed in the laser braze-welding process at different conditions to optimize the process parameters.

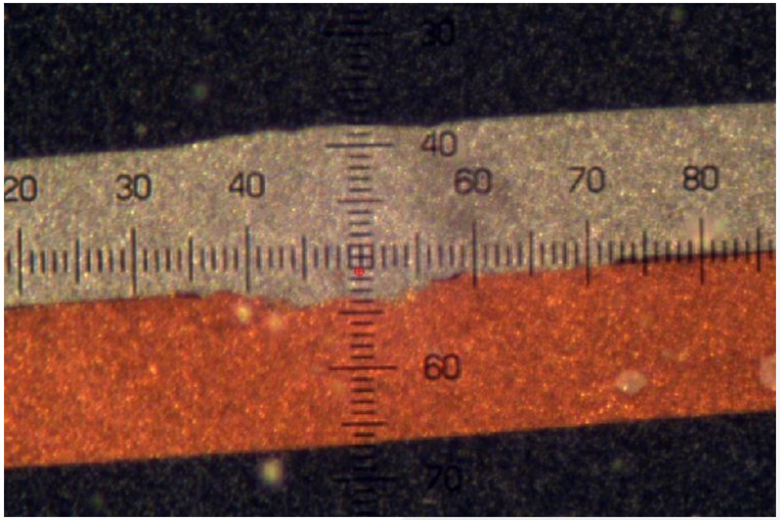

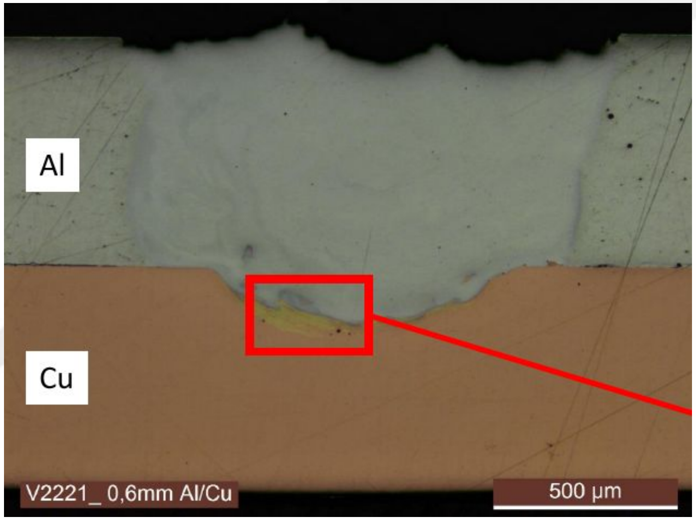

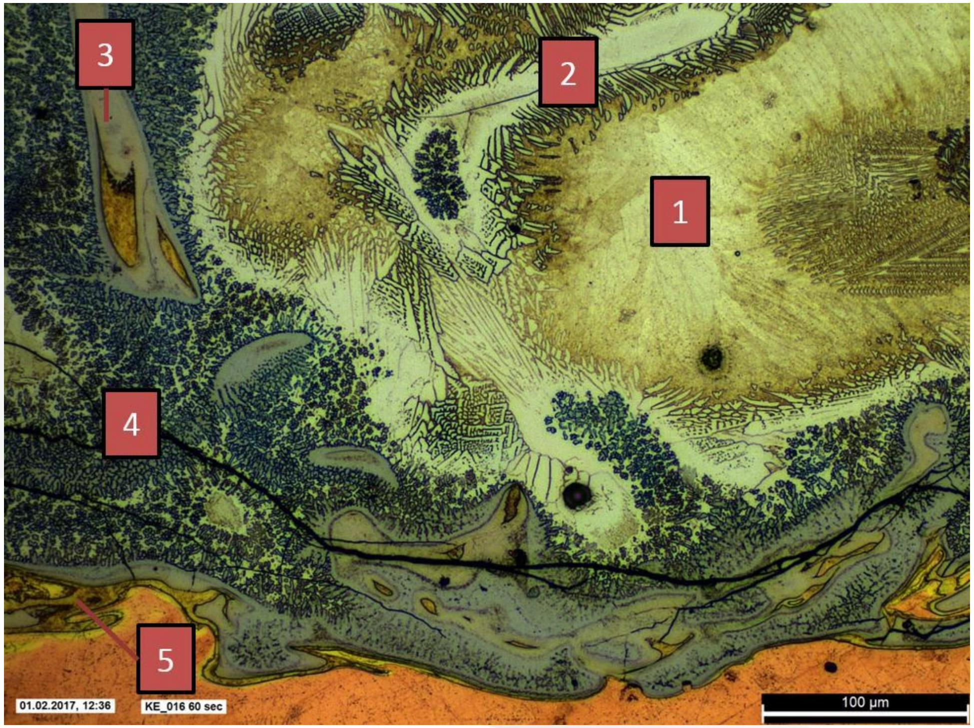

Series of measurements with a small beam size (15x15µm) through the welding joint (transmission)

Schmalen, P. *et al*. Investigation of the Intermetallic Structure of Laser Welded Al-Cu Joints. *10th CIRP Conference on Photonic Technologies [LANE 2018]*

Intermetallic phases in Al-Cu joints

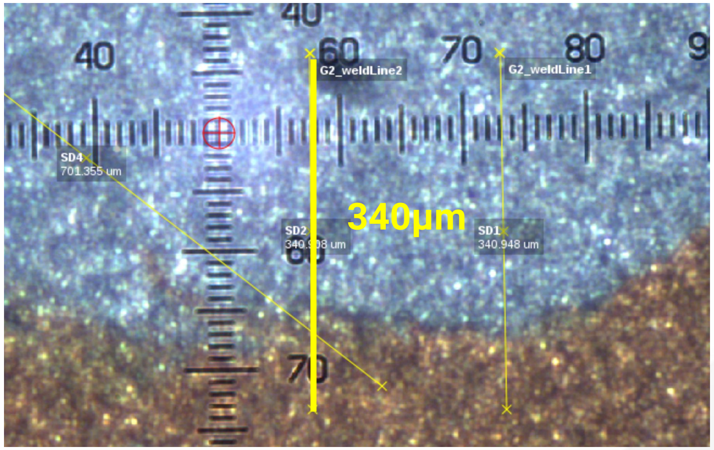

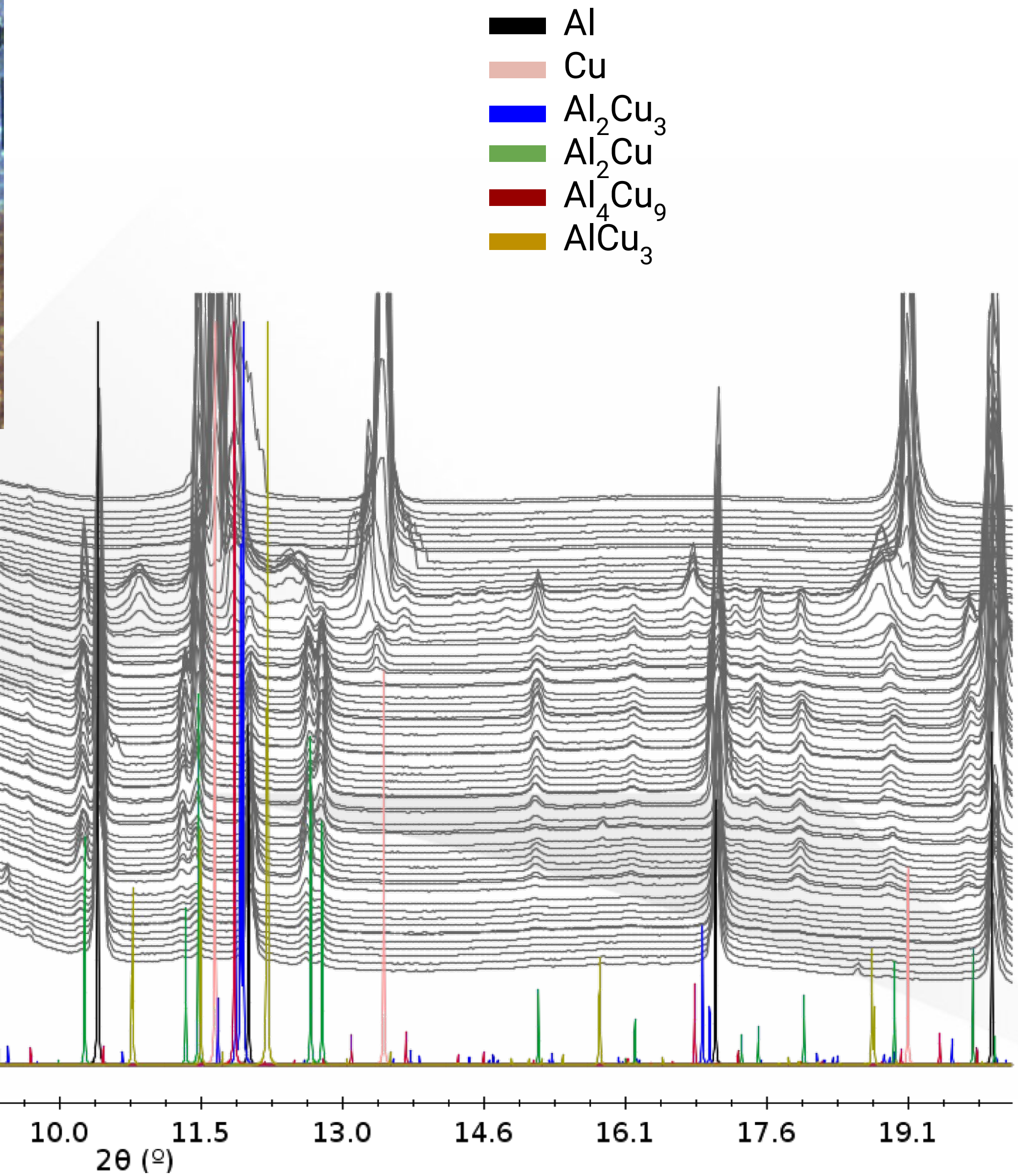

Schmalen, P. *et al*. Investigation of the Intermetallic Structure of Laser Welded Al-Cu Joints. *10th CIRP Conference on Photonic Technologies [LANE 2018]*

Texture study on Nd-Fe-B based nanocomposites

- Measurement in **transmission** to get information on the desired crystallographic axes
- 2D detector for direct texture analysis.

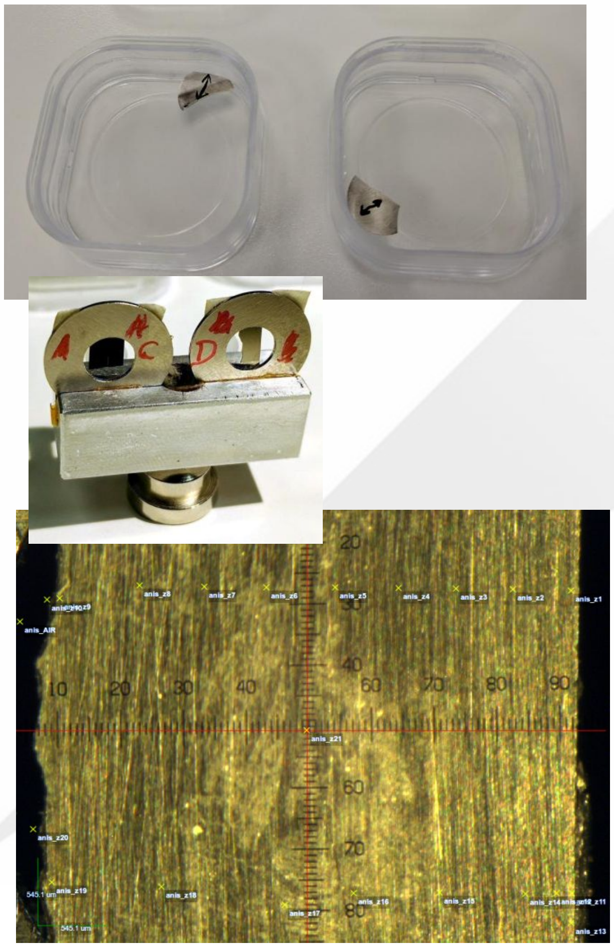

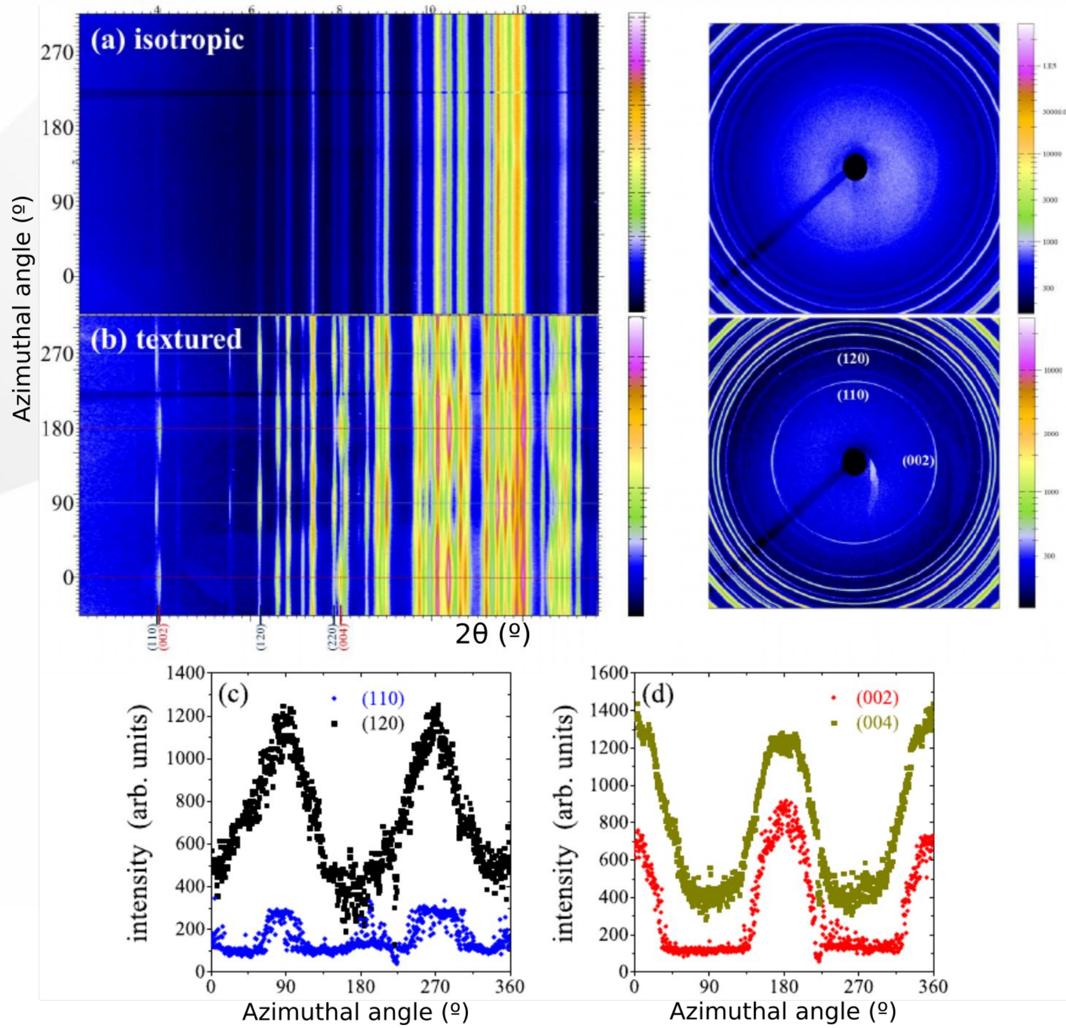

Michels, A. *et al. Chem. Mater.* (2014), 26, 4238−4247

Difracción de polvo y su aplicación en metalurgia

Oriol Vallcorba

Experiments Division
ALBA Synchrotron Light Source - CELLS (www.cells.es)
Carrer de la Llum 2-26, 08290, Cerdanyola del Vallès, Barcelona (Spain)
Phone: +34 93 592 4363 e-mail: ovallcorba@cells.es

Acknowledgements
MSPD Beamline team
ALBA industrial office

Thank you for your attention!

Aplicaciones del Sincrotrón ALBA a la Industria Metalúrgica y al tratamiento de superficies
Cerdanyola del Vallès, June 1st 2018